Vibration control for active magnetic bearing high-speed flywheel-rotor system with inverse system method and two-degree-of-freedom PID control

Chuan MAO, Liangliang CHEN, Changsheng ZHU
College of Electrical Eng., Zhejiang University
310027, Hangzhou, Zhejiang Province, China
E-mail: hello_machine@163.com

Abstract

In the high-speed flywheel energy storage system, the high ratio of the polar to transverse mass moments of inertia of the flywheel rotor and the high operating speed will result in a significant coupled effect. It is not easy to apply normal PID control method in active magnetic bearing (AMB) high-speed flywheel-rotor system for its coupling characteristic. In order to improve the coupled performances of this system, a control strategy that combines inverse system method and two-degree-of-freedom PID control is proposed in this paper. After introducing the model of an AMB high-speed flywheel-rotor system, the decoupling and interference rejection capabilities are simulated. The results show that with by means of the control strategy proposed, the system with strong gyroscopic effect in the high rotating speed region is decoupled and both the static and dynamic performances are greatly improved. An experiment has been done to verify the feasibility of the control strategy proposed.

Keywords : decoupling, magnetic bearing, flywheel, inverse system,2-DOF PID.

1. Introduction

In the flywheel energy storage system, a high-speed flywheel is widely used to store energies. In order to maximize the energy density and storage efficiency, the rotating speed of the flywheel rotor should be as high as possible and the polar moment of inertia of the flywheel rotor should be as large as possible. Active magnetic bearing (AMB) is the best choice for the supporting structure of a high-speed flywheel energy storage system due to its no contact, no wear, no need of lubrication and dynamic adjustable. Therefore, the high-speed flywheel which is supported on active magnetic bearings and made by composite materials is considered as a promising and attracting one. In the high-speed flywheel energy storage system, the high ratio of the polar to transverse mass moments of inertia of the flywheel rotor and the high operating speed will result in a significant coupled effect. The effect greatly increases the complexity of the control system, and may results in rotor instability in some cases. It is not easy to apply normal PID control method in active magnetic bearing (AMB) high-speed flywheel-rotor system for its coupling characteristic. (Ahrens and Kucera, 1996). In order to deal with such rotor instability, it is necessary to develop some advanced control methods.

For stabilizing the high-speed flywheel system with strong gyroscopic effects, various control methods have been presented. They are classified into two kinds, one is based on the traditional decentralized control with cross-feedback (Zhao, et al., 2006), which has a simple structure and good performance, but designing a good controller is not so easily due to the coupling between body modes. The other is based on the modern control theory, such as μ synthesis control (Schönhoff, et al., 2000), sliding mode control (Ann and Raymond, 1996). These control methods can get a good performance, but they are difficult to realize due to the large time-consuming.

In order to improve the coupled performances of this system, a control strategy that combines inverse system method and two-degree-of-freedom PID control is proposed in this paper. After introducing the model of an AMB high-speed flywheel-rotor system, the decoupling and interference rejection capabilities are simulated. The results

show that with by means of the control strategy proposed, the system with strong gyroscopic effect in the high rotating speed region is decoupled and both the static and dynamic performances are greatly improved.

2. The model of radial 4-DOF AMB high-speed flywheel-rotor system

In the most high-speed flywheel energy storage systems, the bending critical speed of the flywheel rotor system is much more than the operating speed, so the flywheel rotor system is often considered as a rigid shaft. Fig. 1 shows the schema of a simplified model of the vertically rigid flywheel rotor system supported by a pair of permanent material(PM) bearings located on the top and bottom sides and radially by two AMBs, the rotor positions are measured by four eddy current-type sensors.

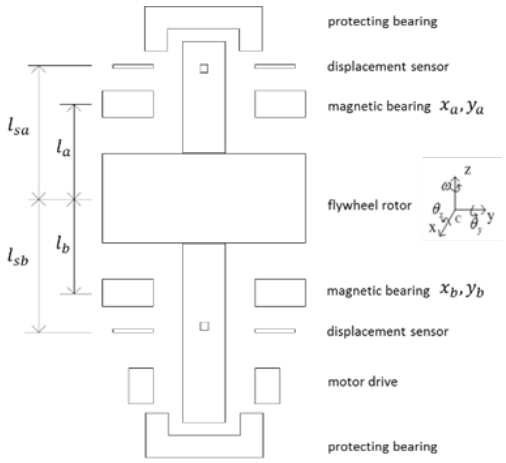

Fig. 1 The model of rigid high-speed flywheel rotor system with AMBs

Based on some assumptions, the equations of motion of flywheel rotor system can be described as

$$\begin{cases} m\ddot{x} = f_{xa} + f_{xb} \\ m\ddot{y} = f_{ya} + f_{yb} \\ J\ddot{\theta}_y - J_z\omega\dot{\theta}_x = f_{xa}l_a - f_{xb}l_b \\ J\ddot{\theta}_x + J_z\omega\dot{\theta}_y = -f_{ya}l_a + f_{yb}l_b \end{cases} \tag{1}$$

where m is the total mass of the flywheel rotor, J_x and J_y are transverse mass moments of inertia of the flywheel rotor around x and y axis ($J_x = J_y = J$), J_z is polar mass moment of inertia of the spinning flywheel rotor around z axis. f_{xa} , f_{xb} , f_{ya} and f_{yb} are magnetic forces acting on the flywheel rotor in the upper and lower radial AMBs.

It can be rewritten as

$$M\ddot{q} + G\dot{q} = L_f u_f \tag{2}$$

where $M = \begin{bmatrix} J & 0 & 0 & 0 \\ 0 & m & 0 & 0 \\ 0 & 0 & J & 0 \\ 0 & 0 & 0 & m \end{bmatrix}$, $q = \begin{bmatrix} \theta_y \\ x \\ \theta_x \\ y \end{bmatrix}$, $G = \begin{bmatrix} 0 & 0 & -J_z\omega & 0 \\ 0 & 0 & 0 & 0 \\ J_z\omega & 0 & 0 & 0 \\ 0 & 0 & 0 & 0 \end{bmatrix}$, $L_f = \begin{bmatrix} l_a & -l_b & 0 & 0 \\ 1 & 1 & 0 & 0 \\ 0 & 0 & -l_b & l_a \\ 0 & 0 & 1 & 1 \end{bmatrix}$, $u_f = \begin{bmatrix} f_{xa} \\ f_{xb} \\ f_{ya} \\ f_{yb} \end{bmatrix}$.

Neglecting the effects of magnetic saturation and leakage, the equations describing the radial suspension forces can be written as

$$\begin{cases} f_{xa} = k_{sa}x_a + k_{ia}i_{xa} \\ f_{xb} = k_{sb}x_b + k_{ib}i_{xb} \\ f_{ya} = k_{sa}y_a + k_{ia}i_{ya} \\ f_{yb} = k_{sb}y_b + k_{ib}i_{yb} \end{cases} \tag{3}$$

where (k_{sa}, k_{ia}) and (k_{sb}, k_{ib}) are force-displacement and force-current coefficients of the upper radial AMB and lower the

radial AMB, respectively.

The matrix form of the magnetic forces acting on the flywheel rotor can be expressed as

$$u_f = K_s \bullet b + K_i \bullet I \tag{4}$$

where $K_s = \begin{bmatrix} k_{sa} & 0 & 0 & 0 \\ 0 & k_{sb} & 0 & 0 \\ 0 & 0 & k_{sa} & 0 \\ 0 & 0 & 0 & k_{sb} \end{bmatrix}$, $K_i = \begin{bmatrix} k_{ia} & 0 & 0 & 0 \\ 0 & k_{ib} & 0 & 0 \\ 0 & 0 & k_{ia} & 0 \\ 0 & 0 & 0 & k_{ib} \end{bmatrix}$.

The two coordinates $(x_a \quad x_b \quad y_a \quad y_b)$ and $(\theta_y \quad x \quad \theta_x \quad y)$ satisfy

$$b = \begin{bmatrix} x_a \\ x_b \\ y_a \\ y_b \end{bmatrix} = \begin{bmatrix} l_a & 1 & 0 & 0 \\ -l_b & 1 & 0 & 0 \\ 0 & 0 & -l_a & 1 \\ 0 & 0 & l_b & 1 \end{bmatrix} \begin{bmatrix} \theta_y \\ x \\ \theta_x \\ y \end{bmatrix} = T_{qb} \bullet q \tag{5}$$

Obviously, $T_{qb} = L_f{}^T$.

Finally, the matrix form of the equations of motion of rigid flywheel rotor system is

$$M\ddot{q} + G\dot{q} = K_{ss} q + L_f K_i I \tag{6}$$

where $K_{ss} = L_f K_s L_f{}^T = \begin{bmatrix} k_{sa} l_a{}^2 + k_{sb} l_b{}^2 & k_{sa} l_a - k_{sb} l_b & 0 & 0 \\ k_{sa} l_a - k_{sb} l_b & k_{sa} + k_{sb} & 0 & 0 \\ 0 & 0 & k_{sa} l_a{}^2 + k_{sb} l_b{}^2 & -k_{sa} l_a + k_{sb} l_b \\ 0 & 0 & -k_{sa} l_a + k_{sb} l_b & k_{sa} + k_{sb} \end{bmatrix}$.

3. Control strategy

Defining state variables $x = [q \quad \dot{q}]^T$, input $u = \begin{bmatrix} i_{xa} & i_{xb} & i_{ya} & i_{yb} \end{bmatrix}^T$, output $y = b = T_{qb} \bullet q$, from Eq. (6), we can obtain

$$\ddot{q} = M^{-1} K_{ss} q - M^{-1} G \dot{q} + M^{-1} L_f K_i I \tag{7}$$

So the state equation of motion of rigid flywheel rotor system can be described as

$$\begin{cases} \dot{x} = Ax + Bu \\ y = Cx \end{cases} \tag{8}$$

where $A = \begin{bmatrix} 0_{4\times4} & I_{4\times4} \\ M^{-1} K_{ss} & -M^{-1} G \end{bmatrix}$, $B = \begin{bmatrix} 0_{4\times4} \\ M^{-1} L_f K_i \end{bmatrix}$, $C = \begin{bmatrix} T_{qb} & 0_{4\times4} \end{bmatrix}$.

Thus

$$\ddot{y} = T_{qb} \bullet \ddot{q} = W_1 x + W_2 u \tag{9}$$

where $W_1 = \begin{bmatrix} T_{qb} M^{-1} K_{ss} & -T_{qb} M^{-1} G \end{bmatrix}$, $W_2 = T_{qb} M^{-1} L_f K_i$.

3.1 Decoupled controller based on inverse system method

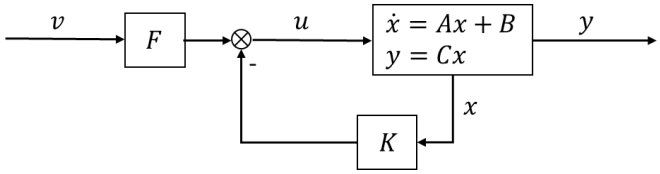

Fig. 2 Block diagram of decoupled controller

As shown in Fig. 2, we design the feedback matrix K and the compensation matrix F to let the system become a decoupled system with integral type. According to the request, output variables y and input variables v satisfy

$$v = \ddot{y} \tag{10}$$

From Eq. (9) and Eq. (10), we obtain

$$v = W_1 x + W_2 u \tag{11}$$

Thus

$$u = -W_2^{-1} W_1 x + W_2^{-1} v \tag{12}$$

Finally, we have

$$\begin{cases} K = -W_2^{-1} W \\ F = W_2^{-1} \end{cases} \tag{13}$$

In which,

$$W_2 = T_{qb} M^{-1} L_f K_i = \begin{bmatrix} \left(\frac{l_a^2}{J} + \frac{1}{m}\right) k_{ia} & \left(-\frac{l_a l_b}{J} + \frac{1}{m}\right) k_{ib} & 0 & 0 \\ \left(-\frac{l_a l_b}{J} + \frac{1}{m}\right) k_{ia} & \left(\frac{l_b^2}{J} + \frac{1}{m}\right) k_{ib} & 0 & 0 \\ 0 & 0 & \left(\frac{l_a^2}{J} + \frac{1}{m}\right) k_{ia} & \left(-\frac{l_a l_b}{J} + \frac{1}{m}\right) k_{ib} \\ 0 & 0 & \left(-\frac{l_a l_b}{J} + \frac{1}{m}\right) k_{ia} & \left(\frac{l_b^2}{J} + \frac{1}{m}\right) k_{ib} \end{bmatrix}$$

$$F = W_2^{-1} = \begin{bmatrix} \frac{m l_b^2 + J}{k_{ia}(l_a + l_b)^2} & \frac{m l_a l_b - J}{k_{ia}(l_a + l_b)^2} & 0 & 0 \\ \frac{m l_a l_b - J}{k_{ib}(l_a + l_b)^2} & \frac{m l_a^2 + J}{k_{ib}(l_a + l_b)^2} & 0 & 0 \\ 0 & 0 & \frac{m l_b^2 + J}{k_{ia}(l_a + l_b)^2} & \frac{m l_a l_b - J}{k_{ia}(l_a + l_b)^2} \\ 0 & 0 & \frac{m l_a l_b - J}{k_{ib}(l_a + l_b)^2} & \frac{m l_a^2 + J}{k_{ib}(l_a + l_b)^2} \end{bmatrix}$$

$$W_1 = \begin{bmatrix} T_{qb} M^{-1} K_{ss} & -T_{qb} M^{-1} G \end{bmatrix} = \begin{bmatrix} M_{11} & 0_{2\times 2} & 0_{2\times 2} & M_{14} \\ 0_{2\times 2} & M_{22} & M_{23} & 0_{2\times 2} \end{bmatrix}$$

$$M_{11} = M_{22} = \begin{bmatrix} \left(\frac{l_a^2}{J} + \frac{1}{m}\right) k_{sa} l_a - \left(-\frac{l_a l_b}{J} + \frac{1}{m}\right) k_{sb} l_b & \left(\frac{l_a^2}{J} + \frac{1}{m}\right) k_{sa} + \left(-\frac{l_a l_b}{J} + \frac{1}{m}\right) k_{sb} \\ \left(-\frac{l_a l_b}{J} + \frac{1}{m}\right) k_{sa} l_a - \left(\frac{l_b^2}{J} + \frac{1}{m}\right) k_{sb} l_b & \left(-\frac{l_a l_b}{J} + \frac{1}{m}\right) k_{sa} + \left(\frac{l_b^2}{J} + \frac{1}{m}\right) k_{sb} \end{bmatrix}$$

$$M_{14} = M_{23} = \begin{bmatrix} \frac{l_a J_z \omega}{J} & 0 \\ -\frac{l_b J_z \omega}{J} & 0 \end{bmatrix}$$

3.2 Feedforward 2-DOF PID controller

In order to achieve a better property of command tracking and disturbance rejection, a 2-DOF feedforward PID controller is proposed. Fig.3 shows the principle of 2-DOF PID control, this kind of 2-DOF PID controller is called setting value feedforward type.

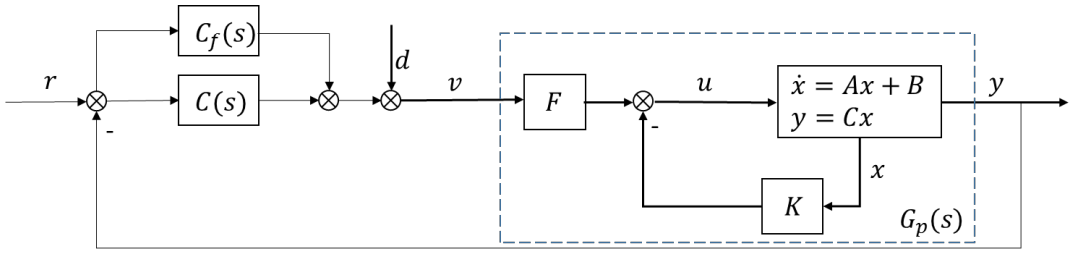

Fig. 3 Block diagram of 2-DOF PID control

From Fig. 3, we obtain

$$\frac{Y(s)}{R(s)} = \frac{\left[C(s)+C_f(s)\right]G_p(s)}{1+G_p(s)C(s)}, \frac{Y(s)}{D(s)} = \frac{G_p(s)}{1+G_p(s)C(s)}.$$

where $G_p(s) = \frac{1}{s^2}$, $C(s) = K_p(1+\frac{1}{T_i s}+T_D s)$, $C_f(s) = -K_p(\alpha+\beta T_D s)$, in which, α and β are coefficients of 2-DOF

From the design principle of the 2-DOF PID controller and the transfer functions, we can draw the conclusions bellow:

(1) $C(s)$ is the control algorithm to restrain interference, the system can achieve its best property of interference restraining by adjusting K_p, T_i, T_D,

(2) $C(s)$ and $C_f(s)$ are the control algorithms to track the setting values, the system can achieve its best property of tracking by adjusting α and β.

4. Analysis of simulation results

The basic parameters of the flywheel rotor supported on AMBs are: total mass of the flywheel rotor $m = 54.3kg$, distance between the rotor mass center and AMBs center $l_a = 277mm, l_b = 250mm$, distance between the rotor mass center and sensors center $l_{sa} = 361mm, l_{sb} = 333mm$, transverse mass moment of inertia of the flywheel rotor system around the x and y axes $J_x = J_y = 1.61kgm^2$, polar mass moment of inertia of the flywheel rotor system around the z axis $J_z = 0.176kgm^2$, radial clearance of the radial AMBs $C_0 = 0.4mm$, current stiffness coefficients of the radial AMBs $k_{ia} = 602.65NA^{-1}, k_{ib} = 578NA^{-1}$, displacement stiffness coefficients of the radial AMBs $k_{sa} = 9.25\times10^5 Nm^{-1}, k_{sb} = 8.875\times10^5 Nm^{-1}$.

4.1 Decoupling

Applying a step signal in x_a at 0.2s when the rotor is static and at a speed of 0 and 20000 rpm, the rotor responses are shown in Fig. 4 and Fig. 5, respectively. It is shown in Fig. 4 that when the rotor is static, coupling between four channels is not strong, the displacement of lower side remain unchanged, but when the rotor speed becomes high(such as 20000rpm), the strong coupling characteristic appears. When using the proposed control strategy, repeat the simulation, the other channels remain unchanged, either the rotor is rotating at a speed of 0 or 20000 rpm. This means that the interference in a certain degree of freedom doesn't influence the others. That is, every degree freedom of the rotor is successfully decoupled with others by the inverse system method proposed.

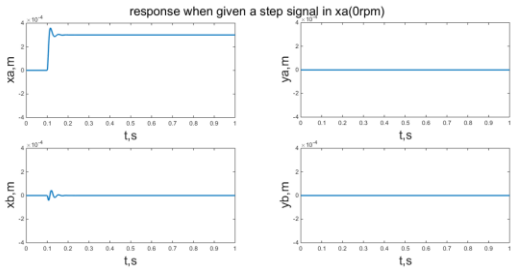

a) at the speed of 0 rpm

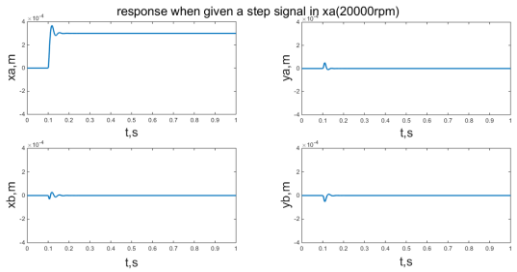

b) at the speed of 20000 rpm

Fig. 4 Responses of each channel when applying a step signal in x_a (decentralized PID control, simulation)

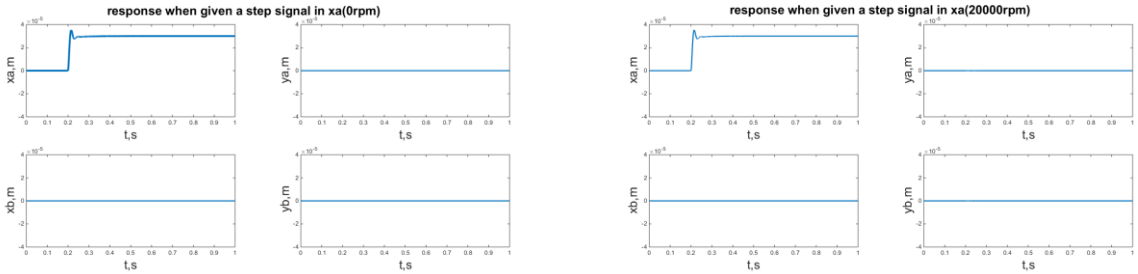

a) at the speed of 0 rpm b) at the speed of 20000 rpm

Fig. 5 Responses of each channel when applying a step signal in x_a (proposed control, simulation)

4.2 Interference rejection capability

For the same interfering signal, the responses using different coefficients of two degree of freedom are shown in Fig. 6. It is shown that the interference rejection capability of the system (including rising time, overshoot and settling time) varies from different coefficients of two degree of freedom. Thus, a better performance of the system by adjusting these two coefficients can be obtained.

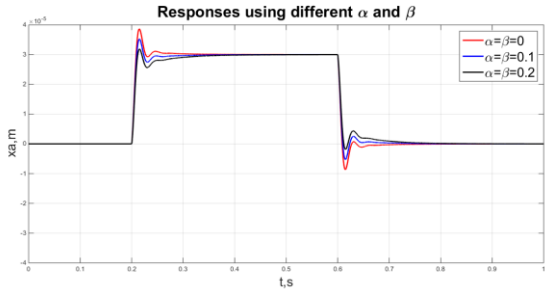

Fig. 6 Responses using different coefficients of 2-DOF

5. Experiment

In order to further observe the ability and effectiveness of the new control method to improve the dynamic characteristics and stability of the AMBs high-speed rigid flywheel rotor system, a series of tests were done in a AMBs flywheel energy storage system with the control strategy proposed. Fig. 7 shows the photos of the AMBs flywheel energy storage system and its flywheel rotor in this experiment.

By using the proposed control method, accelerating a rotor from 0 to 8000 rpm, successfully suspend the rotor during the whole acceleration. Fig. 8 shows the vibration response of the flywheel rotor. The rotor vibrates a little in the low rotating speed region caused by the output voltage fluctuation of Variable-frequency Drive (VDF), it still much less than radial clearance. More significantly, the vibration is even less although the coupled effect appears in the high speed region. It further validates the feasibility of the control strategy proposed.

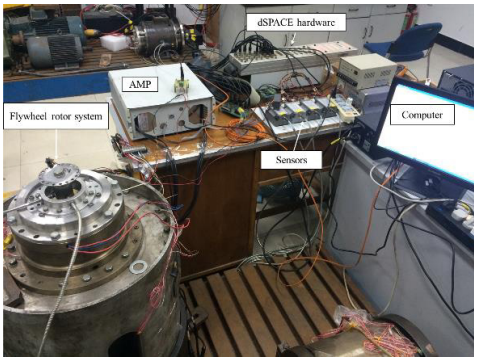

Fig. 7 Experimental platform

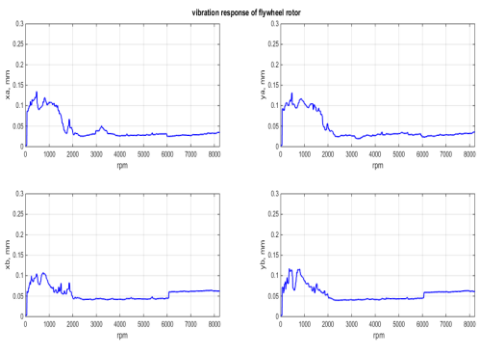

Fig. 8 Vibration response of the flywheel rotor during the acceleration

In order to verify the decoupling performance of the proposed control strategy, an experiment similar to the simulation in section 3 is done. Comparing Fig. 9 and Fig. 10 with Fig. 4 and Fig. 5, it can be seen that the experimental results match the simulation very well. As shown in Fig. 9, the step displacement of channel x_a results in a fluctuation to channel x_b with the traditional controller. However, as shown in Fig. 10, it has little effect on channel x_b with the proposed control strategy. Consequently, the proposed controller achieves the better decoupling performance than the traditional one.

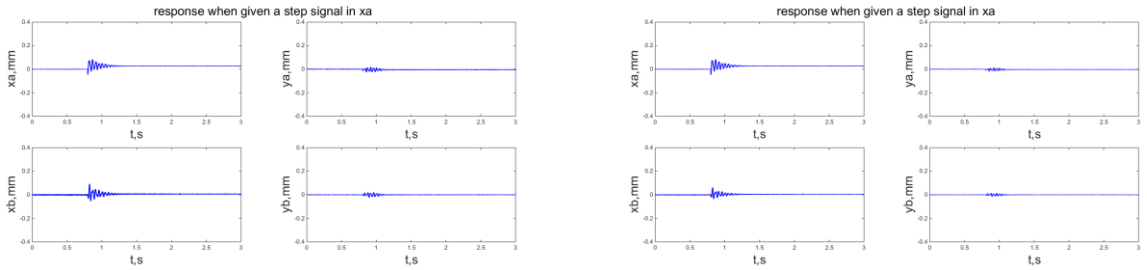

a) at the speed of 0 rpm b) at the speed of 5000 rpm

Fig. 9 Responses of each channel when applying a step signal in x_a (decentralized PID control, experiment)

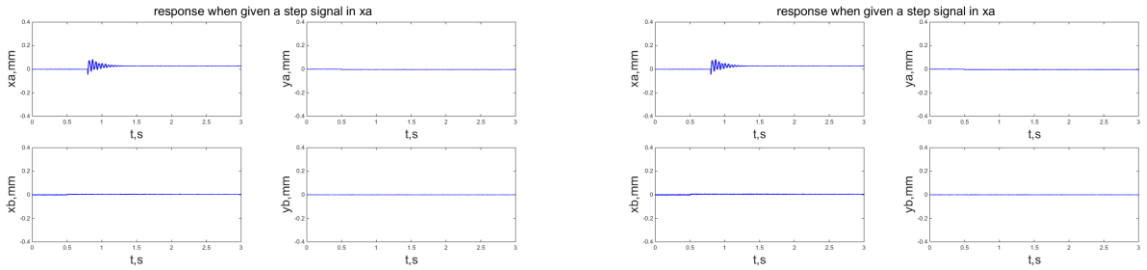

a) at the speed of 0 rpm b) at the speed of 5000 rpm

Fig. 10 Responses of each channel when applying a step signal in x_a (proposed control, experiment)

6. Conclusion

The high-speed flywheel energy storage system is multivariable, highly nonlinear as well as strongly coupling. Comparing with the traditional decentralized PID control, this paper propose a control strategy based on inverse system method and two-degree-of-freedom PID control. By designing the feedback matrix and the compensation matrix, the system can be treated as a decoupled system with integral type. In order to achieve a better property of command tracking and disturbance rejection, a 2-DOF feedforward PID controller was proposed. Simulation and experimental result demonstrate that the proposed strategy has higher decoupling precision, better command tracking, higher disturbance rejection, and stronger robustness performances than the traditional one. Moreover, it can adjust the performances of tracking and disturbance rejection independently.

7. Acknowledgment

This work was sponsored by National Natural Science Foundation of China (51477155、11172261), Natural Science Foundation Project of Zhejiang Province (LZ13E070001), and Project of Collaborative Innovation Center of Advanced Aero-engine.

References

Ahrens, M., and Kucera, L., Performance of a magnetically suspended flywheel energy storage device, IEEE Transaction on Control Systems Technology, Vol.4, No.5 (1996), pp.494–502.

Zhao, L., Zhang, K., and Zhu, R.S., etal, Experimental research on a momentum wheel suspended by active magnetic

bearings, Proceedings of the 8th International Symposium on Magnetic Bearings (2002), pp.605–609.
Schönhoff, U., Luo, J., and Li, G., etal, Implementation results of μ-synthesis control for an energy storage flywheel test rig, Proceedings of the 7th International Symposium on Magnetic Bearings (2000), pp.317–322.
Ann, R., and Raymond, D., A sliding mode observer and controller for stabilization of rotational motion of a vertical shaft magnetic bearing, IEEE Transaction on Control Systems Technology, Vol.4, No.5 (1996), pp.598–608.
Jiancheng Fang and Yuan Ren, Decoupling control of magnetically suspended rotor system in control moment gyros based on an inverse system method, IEEE/ASME Trans. Mechatronics, Vol.17, No.6 (2012), pp.1133–1144.
Shuyun Jiang and Lihua JU, Study on electromechanical coupling nonlinear vibration of flywheel energy storage system, Science in China: Series E Technological Sciences, Vol.49, No.1 (2006), pp.61–77.
Nandi A, Neogy S, Irretier H. Vibration control of a structure and a rotor using one-sided magnetic actuator and a digital proportional-derivative control, Journal of Vibration and Control, Vol.15, No.2 (2009), pp.63–81.